Electronic Supplementary Material (ESI) for Physical Chemistry Chemical Physics.

Electronic Supporting Information: Solvent Effects on the Photoinduced Charge Separation Dynamics of A Directly Linked Zinc Phthalocyanine-Perylenediimide Dyads: A Nonadiabatic Dynamics Simulation with Optimally Tuned Screened Range-Separated Hybrid Functional

Shuai Liu[1], Sha-Sha Liu[1], Xiao-Mei Tang[1], Xiang-Yang Liu[1],* Jia-Jia Yang[1],*

Ganglong Cui[2,3], and Laicai Li[1]*

[1]*College of Chemistry and Material Science, Sichuan Normal University, Chengdu 610068, China and* [2]*Key Laboratory of Theoretical and Computational Photochemistry, Ministry of Education, College of Chemistry, Beijing Normal University, Beijing 100875, China and* [3]*Hefei National Laboratory, Hefei 230088, China*

E-mail: xiangyangliu@sicnu.edu.cn; jiajiayang@sicnu.edu.cn; lilcmail@163.com

Methods

Semi-Classical Absorption Spectra Simulation

Absorption spectra are simulated with a semi-classical method proposed by Barbatti et al.[1,2] On the basis of ground-state ensembles composed of N structures $\mathbf{R}_k$, we can calculate photoabsorption cross section with time-dependent perturbation theory at the first-order level

$$\sigma\left(E\right)=\frac{\pi e^{2}}{2mc\varepsilon_{0}}\sum_{l\neq i}\left[\frac{1}{N}\sum_{k}^{N}f_{il}\left(\mathbf{R}_{k}\right)g\left(E-\Delta E_{il}\left(\mathbf{R}_{k}\right),\delta\right)\right] \tag{S1}$$

where ε_0 is vacuum dielectric constant; c is speed of light; e and m are electron charge and mass; $f_{il}(\mathbf{R}_k)$ and $\Delta E_{il}(\mathbf{R}_k)$ are oscillator strength and transition energy from initial i to final l state at structure $\mathbf{R}_k$; $g\left(E-\Delta E_{il}\left(\mathbf{R}_{k}\right),\delta\right)$ is a normalized line shape function that is peaked at transition energy $\Delta E_{il}(\mathbf{R}_k)$ and broadened by a phenomenological constant δ. In practical applications, there are two kinds of shape functions used to model line shapes. The first one is Gaussian shape function

$$g_{Gauss}\left(E-\Delta E_{il},\delta\right)=\left(\frac{2}{\pi}\right)^{1/2}\frac{\hbar}{\delta}exp\left(\frac{-2\left(E-\Delta E_{il}\right)^{2}}{\delta^{2}}\right) \tag{S2}$$

the second one is Lorentzian shape function

$$g_{Lorentz}\left(E-\Delta E_{il},\delta\right)=\frac{\hbar\delta}{2\pi}\left[\left(E-\Delta E_{il}\right)^{2}+\left(\frac{\delta}{2}\right)^{2}\right]^{-1} \tag{S3}$$

in which $\hbar$ is reduced Planck constant. Our group has recently implemented this method for absorption spectra simulations.[3–6] In the present work, Gaussian shape function is used for simulating absorption spectra from ground to excited state ($i=0$).

Fewest-Switches Surface-Hopping Method

The trajectory-based fewest-switches surface-hopping dynamics simulation approaches by Tully et al.[7] has been extensively employed to simulate a variety of ultrafast excited-state relaxation processes in

chemical/biological systems and materials.[8–16] In the following, a brief presentation is given.

Treating nuclear coordinates $\mathbf{R}(t)$ as variables, the time-dependent electronic Schrödinger equation can be written as

$$i\hbar\dot{\Psi}(\mathbf{r},\mathbf{R}(t),t) = \hat{H}_0(\mathbf{r},\mathbf{R}(t))\Psi(\mathbf{r},\mathbf{R}(t),t) \tag{S4}$$

where $\hat{H}_0(\mathbf{r},\mathbf{R}(t))$ is the zero-order electronic Hamiltonian while $\mathbf{r}$ represents the electronic coordinates. The time-dependent electronic wavefunction is then expressed in terms of a linear combination of adiabatic zero-order electronic spatial wavefunctions:

$$\Psi(\mathbf{r},\mathbf{R}(t),t) = \sum_{i=1}^{N} C_i(t)\Psi_i(\mathbf{r},\mathbf{R}(t)) \tag{S5}$$

in which $\Psi_i(\mathbf{r},\mathbf{R}(t))$ is an eigenfunction of zero-order Hamiltonian $\hat{H}_0(\mathbf{r},\mathbf{R}(t))$ at nuclear coordinates $\mathbf{R}(t)$. Substituting Eq. S5 into Eq. S4, multiplying by $\Psi_j^*(\mathbf{r},\mathbf{R}(t))$ and integrating over the electronic coordinates, we obtain

$$\dot{C}_j(t) = -i\hbar^{-1}C_j(t)E_j(\mathbf{R}(t)) - \sum_{i}^{N} C_i(t)\tau_{ji}(t) \tag{S6}$$

where $\tau_{ji}(t) = \langle\Psi_j|\frac{\partial}{\partial t}\Psi_i\rangle$ is the time derivative nonadiabatic coupling between adiabatic states i and j. $\tau_{ji}(t)$ can also be expressed as $\mathbf{v}(t)\cdot\mathbf{d}_{ji}(\mathbf{R}(t))$ in which $\mathbf{v}(t)$ and $\mathbf{d}_{ji}(\mathbf{R}(t))$ are the nuclear velocities and the adiabatic derivative couplings, respectively. Thus, Eq. S6 can also be written as

$$\dot{C}_j(t) = -i\hbar^{-1}C_j(t)E_j^0(\mathbf{R}(t)) - \sum_{i}^{N} C_i(t)\mathbf{v}(t)\cdot\mathbf{d}_{ji}(\mathbf{R}(t)) \tag{S7}$$

which is the central equation of the fewest-switches surface-hopping method and may describe radiationless transitions between electronic states with the same spin. The fewest-switches criterion finally yields the transition probability from state i to j as

$$p_{ij}(t)dt = 2\frac{\mathrm{Re}(C_i^*C_j\tau_{ij})}{C_i^*C_i}dt \tag{S8}$$

This method has been implemented in our own GTSH package[17] and widely used to simulation photoinduced ultrafast processes of molecular, biological and materials systems.[18–23]

Time-Derivative Nonadiabatic Couplings

The time derivative nonadiabatic couplings $\tau_{ji}(t)$ can be calculated from the adiabatic derivative couplings $\mathbf{d}_{ji}(\mathbf{R}(t))$ and the nuclear velocities $\mathbf{v}(t)$, and there are also some analytical expressions for $\mathbf{d}_{ji}(\mathbf{R}(t))$.[24–26] In addition, there are two types of numerical algorithms available to directly compute $\tau_{ji}(t)$ in the framework of LR-TDDFT.[27,28] Our present work uses the recently developed algorithm. A brief presentation is given below, in which the subscripts $\{a, b, c\}$ denote the virtual orbitals, $\{i, j, k\}$ the occupied orbitals, and $\{p, q, r\}$ for any type of orbitals.

In LR-TDDFT the total electronic wave function of an electronically excited state Ψ_K is approximately written as a linear combination of singly-excited Slater determinants,

$$\Psi_K = \sum_{i}^{occ} \sum_{a}^{unocc} w_{ia}^{K} \psi_i^a \tag{S9}$$

in which w_{ia}^K is the coefficient of the singly-excited Slater determinant ψ_i^a. The determinant $\psi_i^a = \hat{a}_a^\dagger \hat{a}_i \psi_0$ is constructed through the electronic excitation (substitution) operation of the ground-state determinant ψ_0. Thereby, the time derivative nonadiabatic coupling $\tau_{KJ} = \langle \Psi_K | \frac{\partial}{\partial t} \Psi_J \rangle$, can be further written as

$$\tau_{KJ} = \sum_{ijab} \left(w_{ia}^{K*} \partial_t w_{jb}^J \left\langle \psi_i^a \middle| \psi_j^b \right\rangle + w_{ia}^{K*} w_{jb}^J \left\langle \psi_i^a \middle| \partial_t \psi_j^b \right\rangle \right) \tag{S10}$$

The first term simplifies to $\sum_{ia} w_{ia}^{K*} \partial_t w_{ia}^J$ due to the orthogonality condition for the molecular orbitals (MOs) $\langle \phi_p | \phi_q \rangle = \delta_{pq}$. The time differentiation on ψ_j^b gives

$$\partial_t \psi_j^b = \sum_{k \neq j} \psi_j^b \{k\}' + \psi_j^{b'} \tag{S11}$$

where $\psi_p^q \{r\}'$ denotes a determinant originated from ψ_p^q but with the MO ϕ_r ($r \neq p$) replaced by its time derivative $\partial_t \phi_r$, and $\psi_p^{q'}$ denotes a determinant originated from ψ_p^q but with the MO ϕ_p replaced

by the time derivative $\partial_t \phi_q$. Therefore, the 2nd term in formula S10 becomes

$$\left\langle \psi_i^a \left| \partial_t \psi_j^b \right. \right\rangle = \sum_{k \neq j} \left\langle \psi_i^a \left| \psi_{jk}^{bk'} \right. \right\rangle + \left\langle \psi_i^a \left| \psi_j^{b'} \right. \right\rangle \tag{S12}$$

in which the last term above is reduced to $\delta_{ij} \left\langle \phi_a \left| \partial_t \phi_b \right. \right\rangle$, while only one term with $k = i$ and $a = b$ from sum over k survives due to orthogonality conditions ($\left\langle \phi_p \left| \partial_t \phi_p \right. \right\rangle = 0$ for real orbitals; $\left\langle \phi_p \left| \phi_q \right. \right\rangle = \delta_{pq}$). Then, we arrive at

$$\left\langle \psi_i^a \left| \partial_t \psi_j^b \right. \right\rangle = \delta_{ij} \left\langle \phi_a \left| \partial_t \phi_b \right. \right\rangle - P_{ij} \delta_{ab} \left\langle \phi_j \left| \partial_t \phi_i \right. \right\rangle \tag{S13}$$

where P_{ij} is an additional phase factor that depends on the ordering convention for the orbitals used in the Slater determinants.

Finally, the computational expression for the time derivative nonadiabatic couplings is written as

$$\tau_{KJ} = \sum_{ia} w_{ia}^K \partial_t w_{ia}^J + \sum_{iab} w_{ia}^K w_{ib}^J \left\langle \phi_a \left| \partial_t \phi_b \right. \right\rangle - \sum_{ija} P_{ij} w_{ia}^K w_{ja}^J \left\langle \phi_j \left| \partial_t \phi_i \right. \right\rangle \tag{S14}$$

in which the terms related to the time derivatives of MOs can be calculated using a finite-difference scheme

$$\left\langle \phi_p \left| \partial_t \phi_q \right. \right\rangle = \frac{1}{\Delta t} \left\langle \phi_p \left(t \right) \left| \phi_q \left(t + \Delta t \right) \right. \right\rangle \tag{S15}$$

where $\phi_p \left(t \right)$ and $\phi_q \left(t + \Delta t \right)$ represent MOs at t and $t + \Delta t$ times, respectively. The corresponding algorithm has been independently coded into a standalone module in our developed GTSH package.[4–6]

Fragment-Based Exciton Analysis

There are several analysis methods capable of examining the excited-state characters, intra- and inter-molecular electron and energy transfers of complex systems and in particular the donor-acceptor systems. One of the most popular methods is based on analyzing one-electron transition density matrices, which can be implemented in different atomic orbital representations, e.g. nonorthogonal atomic orbitals[29] or Löwdin orthogonalized atomic orbitals.[30] Recently we have implemented a similar analysis method using

Löwdin orthogonalized atomic orbital representation.[3] Within such, the one-electron transition density matrix $\mathbf{T}_{LO}$ is expressed as

$$\mathbf{T}_{\mathrm{LO}} = (\mathbf{S}_{\mathrm{AO}})^{1/2}\,\mathbf{T}_{\mathrm{AO}}\,(\mathbf{S}_{\mathrm{AO}})^{1/2} = (\mathbf{S}_{\mathrm{AO}})^{1/2}\left(\mathbf{C}\mathbf{T}_{\mathrm{MO}}\mathbf{C}^{\mathrm{T}}\right)(\mathbf{S}_{\mathrm{AO}})^{1/2} \tag{S16}$$

where $\mathbf{C}$ and $\mathbf{S}_{AO}$ are the MO coefficients and AO overlap matrices, and $\mathbf{T}_{AO}$ and $\mathbf{T}_{MO}$ represent the one-electron transition density matrices in the AO and MO representations, respectively. Due to the orthogonal property of Löwdin atomic orbitals, the transition contribution from atom a to b becomes

$$D_{ab} = \sum_{i\in a, j\in b} (\mathbf{T}_{\mathrm{LO}})^2_{ij} \tag{S17}$$

where i and j are the indices of the atomic orbitals, and a and b are the indices of the atoms. Thus, transition contribution from a fragment D to another fragment A in a system is given by

$$\Omega_{DA} = \sum_{a\in D, b\in A} D_{ab} \tag{S18}$$

in which $D = A$ and $D \neq A$ represent the local excitation (LE) within fragment D and the charge transfer (CT) excitation from D to A, respectively. Accordingly, contributions of LE and CT to an excited state of interest can be quantitatively obtained. These Ω_{DA} can also be regarded as weights of different fragment-based LE and CT excitons. Moreover, time-dependent electron and hole counts on a fragment can also be calculated.[4–6] The hole count on a fragment D, as a result of electron transfer from D to all fragments A, is computed as

$$h_D = \sum_{a\in D} D_{ab} = \sum_{A} \Omega_{DA} \tag{S19}$$

while, the electron count of a fragment A transferred from all fragments D is defined as

$$e_A = \sum_{b\in A} D_{ab} = \sum_{D} \Omega_{DA} \tag{S20}$$

Electron-Hole Density

Electronic excitation always results in many pairs of hole and electron, which are represented as singly excited Slater determinants ψ_i^a in LR-TDDFT calculations (see above). These electron-hole pairs can be described by occupied and unoccupied MO indices. However, such kind of analysis could be complex if many pairs of MOs are involved. Instead, analyzing spatial distribution of electron and hole produced by all pairs of involved MOs is more useful. In such scheme, hole and electron densities are written as follows[31,32]

$$\rho^{hole}(\mathbf{r}) = \rho_{loc}^{hole}(\mathbf{r}) + \rho_{cross}^{hole}(\mathbf{r}) = \sum_{i\to a}(w_{ia})^2 \phi_i(\mathbf{r})\phi_i(\mathbf{r}) + \sum_{i\to a}\sum_{j\neq i\to a} w_{ia}w_{ja}\phi_i(\mathbf{r})\phi_j(\mathbf{r}) \quad \text{(S21)}$$

$$\rho^{electron}(\mathbf{r}) = \rho_{loc}^{electron}(\mathbf{r}) + \rho_{cross}^{electron}(\mathbf{r}) = \sum_{i\to a}(w_{ia})^2 \phi_a(\mathbf{r})\phi_a(\mathbf{r}) + \sum_{i\to a}\sum_{i\to b\neq a} w_{ia}w_{ib}\phi_a(\mathbf{r})\phi_b(\mathbf{r}) \quad \text{(S22)}$$

in which $\sum_{i\to a} \equiv \sum_i^{occ}\sum_a^{vir}$ and $\sum_{i\to a}\sum_{j\neq i\to a} \equiv \sum_i^{occ}\sum_{j\neq i}^{occ}\sum_a^{vir}$; w_{ia} is coefficient of excited Slater determinant ψ_i^a in an electronically excited electronic state; $\phi_i(\mathbf{r})$ and $\phi_j(\mathbf{r})$ are MOs that hole occupies; $\phi_a(\mathbf{r})$ and $\phi_b(\mathbf{r})$ are MOs that electron occupies. In these equations, the first and second terms stand for contributions of local and cross terms. It is clear that these two electron and hole densities satisfy $\int \rho^{hole}(\mathbf{r})\,d\mathbf{r} = 1$ and $\int \rho^{electron}(\mathbf{r})\,d\mathbf{r} = 1$ due to orthonormality properties of MOs and total sum of squares of all configuration coefficients is 1.0, which means that only one electron is excited leaving one hole. On the basis of electron and hole densities, useful parameters to characterize electron-hole separation can be defined, such as distance of centroids of electron and hole.

Based on density distributions of hole and electron, centroids of hole and electron can be calculated to approximately represent positions of hole and electron. In such case, centroid coordinates X, Y, and Z of electron can be calculated as

$$X_{electron} = \int x\rho^{electron}(\mathbf{r})\, d\mathbf{r} \tag{S23}$$

$$Y_{electron} = \int y\rho^{electron}(\mathbf{r})\, d\mathbf{r} \tag{S24}$$

$$Z_{electron} = \int z\rho^{electron}(\mathbf{r})\, d\mathbf{r} \tag{S25}$$

where x, y, and z are Cartesian coordinate components of electron. Similarly, one can define those for hole.

Additional Figures and Table

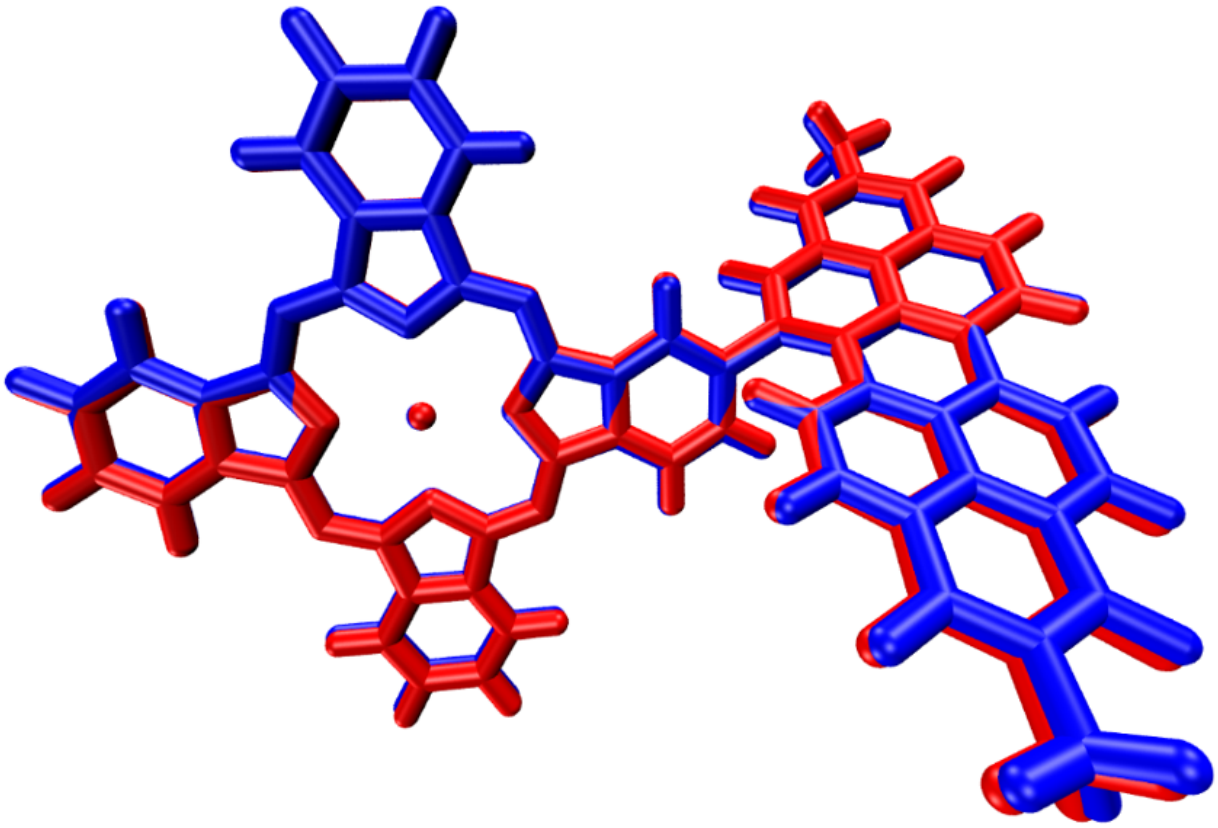

Figure S1: Spatial overlap of the minimum energy structures of ZnPc-PDI dyads optimized with (red) and without (blue) dispersion correction.

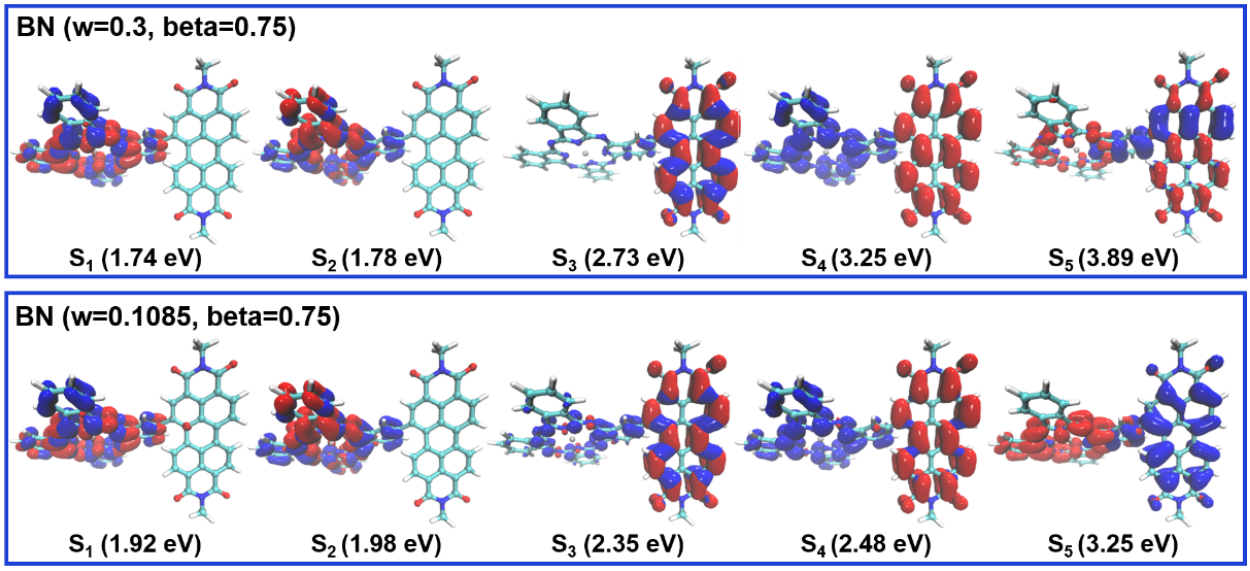

Figure S2: TD-LC-PBE0 calculated photoinduced electron (in red) and hole (in blue) densities of the lowest five singlet excited states of ZnPc-PDI with default (top) and optimally tuned (bottom) ω parameter in gas while the β parameter keeps its original value.

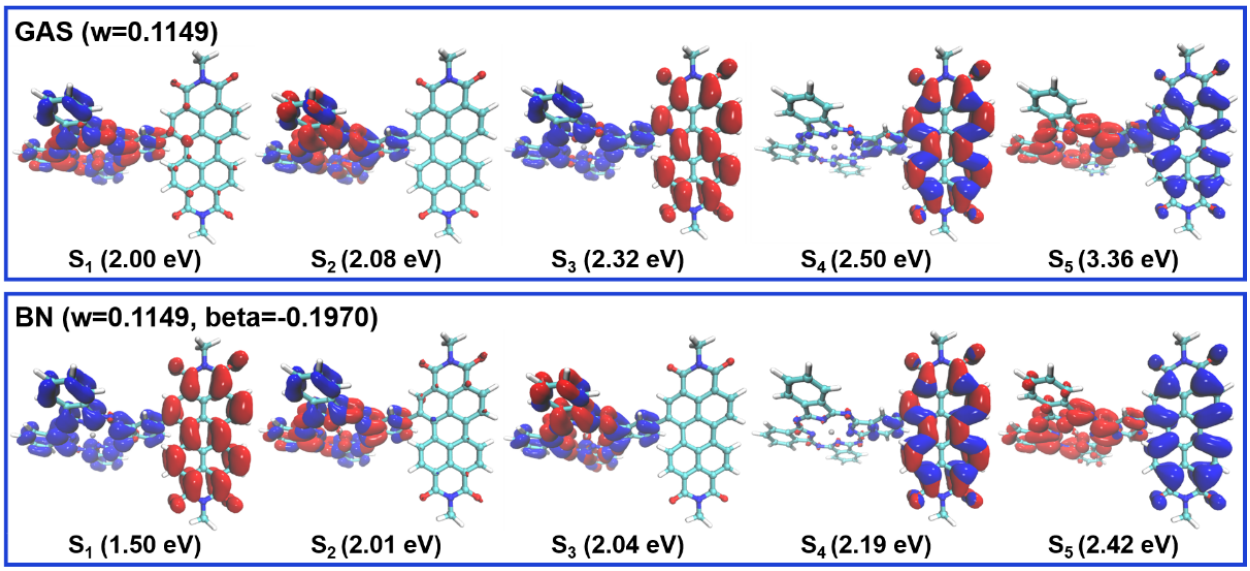

Figure S3: TD-ωB97XD* computed photoinduced electron (electron accumulation, red) and hole (electron depletion, blue) densities of the lowest lying five singlet excited states of the ZnPc-PDI dyads at the Franck-Condon point in gas (top) and benzonitrile (bottom). Also shown are their corresponding vertical excitation energies.

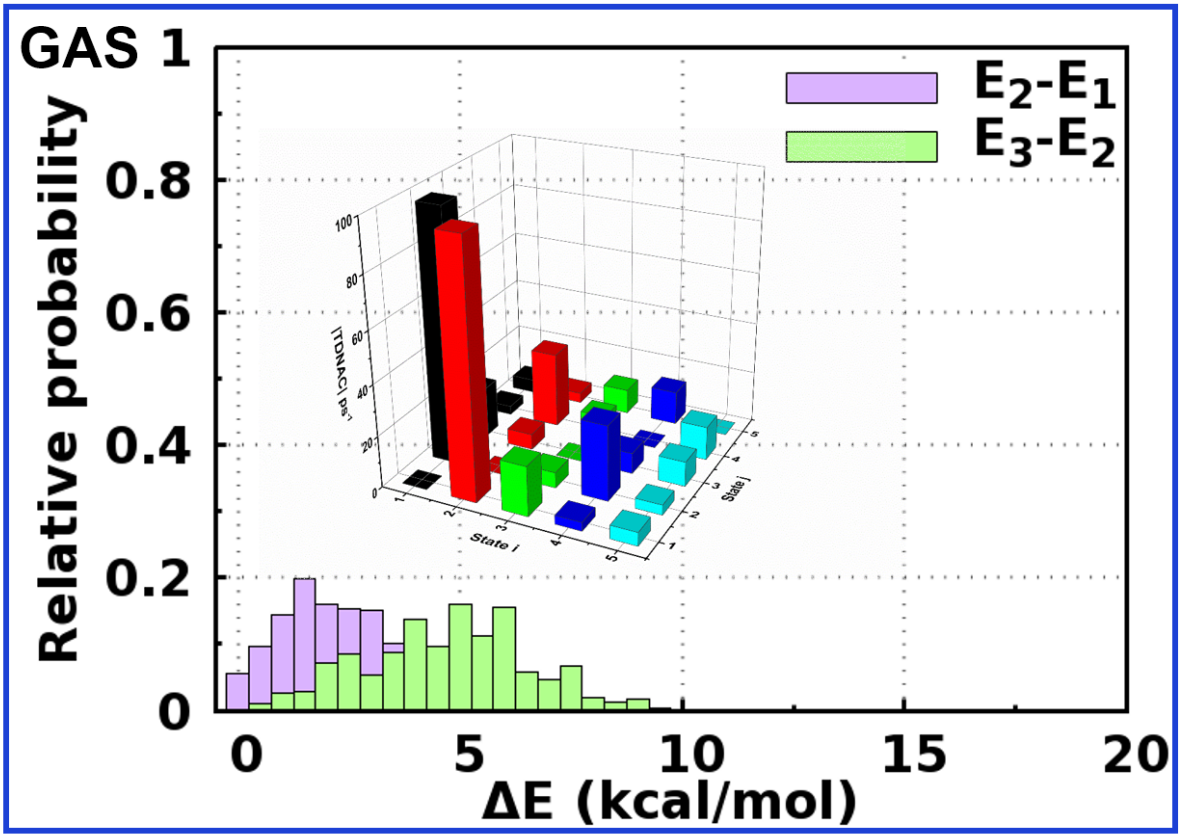

Figure S4: Distribution of energy differences between adjacent states (S_2–S_1, kcal·mol^{-1}) and averaged absolute value of time-derivative nonadiabatic couplings (ps$^{-1)}$ between pairs of related excited states of ZnPc–PDI dyads in gas.

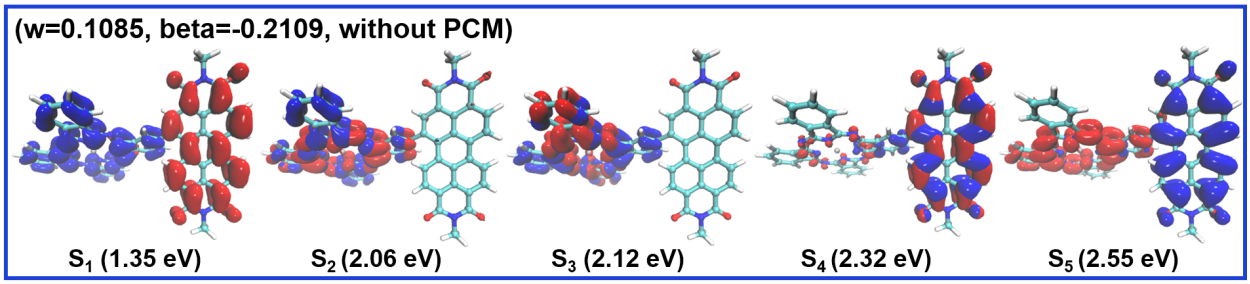

Figure S5: TD-LC-PBE0 calculated photoinduced electron (in red) and hole (in blue) densities of the lowest five singlet excited states of ZnPc–PDI with optimally tuned ω parameter in gas while the β parameter in benzonitrile is obtained using the OT-SRSH procedure without applying PCM model.

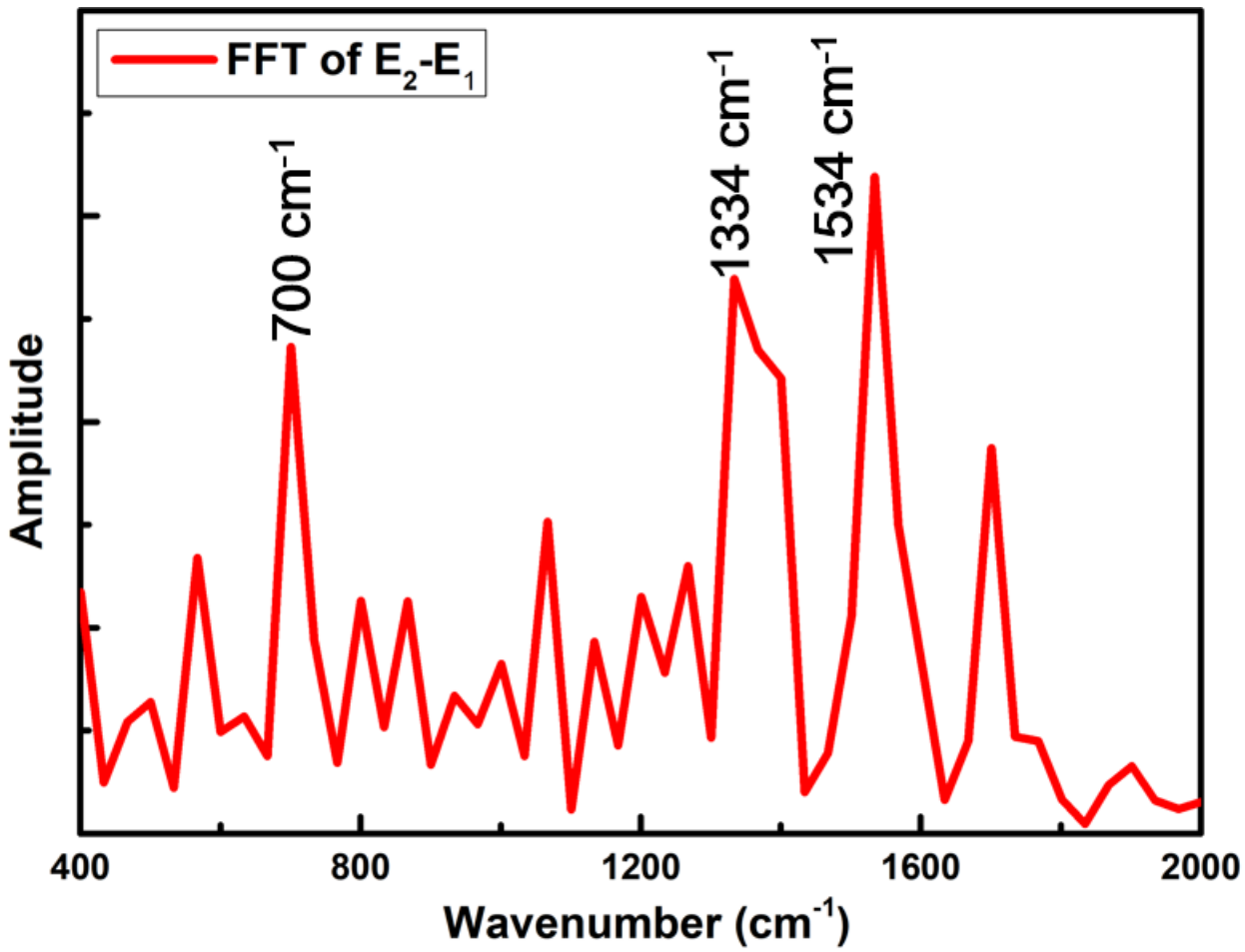

Figure S6: The Fourier transformation of the relevant time dependent energy differences between S_2 and S_1 that is relevant to the charge transfer dynamics in benzonitrile.

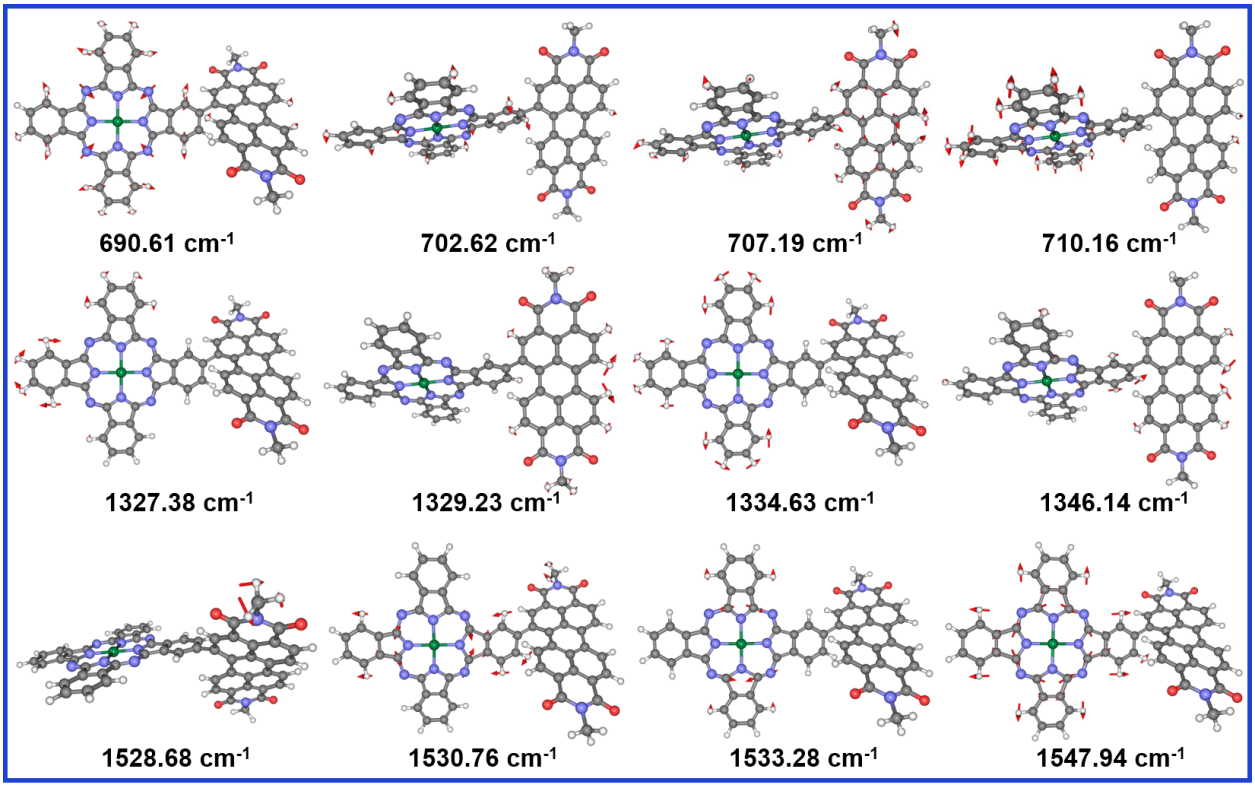

Figure S7: The vibrational normal modes that might play significant roles for the charge transfer dynamics.

References

(1) Barbatti, M.; Aquino, A. J. A.; Lischka, H. The UV Absorption of Nucleobases: Semi-Classical Ab Initio Spectra Simulations. *Phys. Chem. Chem. Phys.* **2010**, *12*, 4959–4967.

(2) Crespo-Otero, R.; Barbatti, M. Spectrum Simulation and Decomposition with Nuclear Ensemble: Formal Derivation and Application to Benzene, Furan and 2-Phenylfuran. *Theor. Chem. Acc.* **2012**, *131*, 1237.

(3) Liu, X.-Y.; Xie, X.-Y.; Fang, W.-H.; Cui, G. L. Photoinduced Relaxation Dynamics of Nitrogen-Capped Silicon Nanoclusters: a TD-DFT study. *Mol. Phys.* **2018**, *116*, 869–884.

(4) Liu, X.-Y.; Li, Z.-W.; Fang, W.-H.; Cui, G. L. Nonadiabatic Dynamics Simulations on Internal Conversion and Intersystem Crossing Processes in Gold(I) Compounds. *J. Chem. Phys.* **2018**, *149*, 044301.

(5) Liu, X.-Y.; Zhang, Y.-H.; Fang, W.-H.; Cui, G. L. Early-Time Excited-State Relaxation Dynamics of Iridium Compounds: Distinct Roles of Electron and Hole Transfer. *J. Chem. Phys. A* **2018**, *122*, 5518–5532.

(6) Fang, Y.-G.; Peng, L.-Y.; Liu, X.-Y.; Fang, W.-H.; Cui, G. L. QM/MM Nonadiabatic Dynamics Simulation on Ultrafast Excited-State Relaxation in Osmium(II) Compounds in Solution. *Comput. Theor. Chem.* **2019**, *1155*, 90–100.

(7) Hammes-Schiffer, S.; Tully, J. C. Proton Transfer in Solution: Molecular Dynamics with Quantum Transitions. *J. Chem. Phys.* **1994**, *101*, 4657–4667.

(8) Barbatti, M.; Aquino, A. J. A.; Szymczak, J. J.; Nachtigallová, D.; Hobza, P.; Lischka, H. Relaxation Mechanisms of UV-Photoexcited DNA and RNA Nucleobases. *Proc. Natl. Acad. Sci. U. S. A.* **2010**, *107*, 21453–21458.

(9) Lu, Y.; Lan, Z. G.; Thiel, W. Hydrogen Bonding Regulates the Monomeric Nonradiative Decay of Adenine in DNA Strands. *Angew. Chem. Int. Ed.* **2011**, *50*, 6864–6867.

(10) Long, R.; English, N. J.; Prezhdo, O. V. Photo-Induced Charge Separation across the Graphene-TiO_2 Interface Is Faster Than Energy Losses: A Time-Domain ab Initio Analysis. *J. Am. Chem. Soc.* **2012**, *134*, 14238–14248.

(11) Fazzi, D.; Barbatti, M.; Thiel, W. Unveiling the Role of Hot Charge-Transfer States in Molecular Aggregates via Nonadiabatic Dynamics. *J. Am. Chem. Soc.* **2016**, *138*, 4502–4511.

(12) Fischer, S. A.; Chapman, C. T.; Li, X. S. Surface Hopping with Ehrenfest Excited Potential. *J. Chem. Phys.* **2011**, *135*, 144102.

(13) Fischer, S. A.; Lingerfelt, D. B.; May, J. W.; Li, X. S. Non-Adiabatic Molecular Dynamics Investigation of Photoionization State Formation and Lifetime in Mn^{2+}-Doped ZnO Quantum Dots. *Phys. Chem. Chem. Phys.* **2014**, *16*, 17507–17514.

(14) Nelson, T.; Fernandez-Alberti, S.; Roitberg, A. E.; Tretiak, S. Nonadiabatic Excited-State Molecular Dynamics: Modeling Photophysics in Organic Conjugated Materials. *Acc. Chem. Res.* **2014**, *47*, 1155–1164.

(15) Richter, M.; Marquetand, P.; González-Vázquez, J.; Sola, I.; González, L. SHARC: ab Initio Molecular Dynamics with Surface Hopping in the Adiabatic Representation Including Arbitrary Couplings. *J. Chem. Theory Comput.* **2011**, *7*, 1253–1258.

(16) Richter, M.; Marquetand, P.; González-Vázquez, J.; Sola, I.; González, L. Femtosecond Intersystem Crossing in the DNA Nucleobase Cytosine. *J. Phys. Chem. Lett.* **2012**, *3*, 3090–3095.

(17) Cui, G. L.; Thiel, W. Generalized Trajectory Surface-Hopping Method for Internal Conversion and Intersystem Crossing. *J. Chem. Phys.* **2014**, *141*, 124101.

(18) Wang, Y.-T.; Liu, X.-Y.; Cui, G. L.; Fang, W.-H.; Thiel, W. Photoisomerization of Arylazopyrazole Photoswitches: Stereospecific Excited-State Relaxation. *Angew. Chem. Int. Ed.* **2016**, *55*, 14009–14013.

(19) Wang, Y.-T.; Gao, Y.-J.; Wang, Q.; Cui, G. L. Photochromic Mechanism of a Bridged Diarylethene: Combined Electronic Structure Calculations and Nonadiabatic Dynamics Simulations. *J. Phys. Chem. A* **2017**, *121*, 793–802.

(20) Xia, S.-H.; Xie, B.-B.; Fang, Q.; Cui, G. L.; Thiel, W. Excited-State Intramolecular Proton Transfer to Carbon Atoms: Nonadiabatic Surface-Hopping Dynamics Simulations. *Phys. Chem. Chem. Phys.* **2015**, *17*, 9687–9697.

(21) Xia, S.-H.; Cui, G. L.; Fang, W.-H.; Thiel, W. How Photoisomerization Drives Peptide Folding and Unfolding: Insights from QM/MM and MM Dynamics Simulations. *Angew. Chem. Int. Ed.* **2016**, *55*, 2067–2072.

(22) Zhang, Y. H.; Sun, X. W.; Zhang, T. S.; Liu, X. Y.; Cui, G. L. Nonadiabatic Dynamics Simulations on Early-Time Photochemistry of Spirobenzopyran. *J. Phys. Chem. A* **2020**, *124*, 2547–2559.

(23) Gao, Y.-J.; Chang, X.-P.; Liu, X.-Y.; Li, Q.-S.; Cui, G. L.; Thiel, W. Excited-State Decay Paths in Tetraphenylethene Derivatives. *J. Phys. Chem. A* **2017**, *121*, 2572–2579.

(24) Send, R.; Furche, F. First-Order Nonadiabatic Couplings from Time-Dependent Hybrid Density Functional Response Theory: Consistent Formalism, Implementation, and Performance. *J. Chem. Phys.* **2010**, *132*, 044107.

(25) Li, Z.; Liu, W. First-Order Nonadiabatic Coupling Matrix Elements between Excited States: A Lagrangian Formulation at the CIS, RPA, TD-HF, and TD-DFT Levels. *J. Chem. Phys.* **2014**, *141*, 014110.

(26) Li, Z.; Suo, B.; Liu, W. First Order Nonadiabatic Coupling Matrix Elements between Excited States: Implementation and Application at the TD-DFT and pp-TDA Levels. *J. Chem. Phys.* **2014**, *141*, 244105.

(27) Pittner, J.; Lischka, H.; Barbatti, M. Optimization of Mixed Quantum-Classical Dynamics: Time-Derivative Coupling Terms and Selected Couplings. *Chem. Phys.* **2009**, *356*, 147–152.

(28) Ryabinkin, I. G.; Nagesh, J.; Izmaylov, A. F. Fast Numerical Evaluation of Time-Derivative Nonadiabatic Couplings for Mixed Quantum-Classical Methods. *J. Phys. Chem. Lett.* **2015**, *6*, 4200–4203.

(29) Plasser, F.; Lischka, H. Analysis of Excitonic and Charge Transfer Interactions from Quantum Chemical Calculations. *J. Chem. Theory Comput.* **2012**, *8*, 2777–2789.

(30) Huang, J.; Du, L.; Hu, D.; Lan, Z. G. Theoretical Analysis of Excited States and Energy Transfer Mechanism in Conjugated Dendrimers. *J. Comput. Chem.* **2015**, *36*, 151–163.

(31) Lu, T.; Chen, F. Multiwfn: A Multifunctional Wavefunction Analyzer. *J. Comput. Chem.* **2012**, *33*, 580–592.

(32) Liu, Z. Y.; Lu, T.; Chen, Q. X. An Sp-Hybridized All-Carboatomic Ring, Cyclo 18 Carbon: Electronic Structure, Electronic Spectrum, and Optical Nonlinearity. *Carbon* **2020**, *165*, 461–467.

Cartesian Coordinates (in xyz format)

101

ZnPc-PDI

C	15.25553740	-4.07588030	3.31641934
C	17.01855681	-4.36077794	1.94513504
C	14.85226693	-3.57058376	2.00421403
C	15.95845180	-3.74930952	1.14391688
C	13.66501411	-3.00475012	1.54203007
C	15.89877706	-3.36548725	-0.19485913
C	13.60692569	-2.62092759	0.20131031
H	12.82093348	-2.87241134	2.21149771
C	14.70935790	-2.79900119	-0.65595098
H	16.75479868	-3.50750282	-0.84694697
H	12.69616714	-2.17668559	-0.19073949
H	14.62970963	-2.48898708	-1.69425075
C	19.22881445	-6.92959280	8.33021020
C	20.33464218	-7.10790828	7.46956897
C	21.52203057	-7.67605292	7.92751779
C	21.60351466	-8.05605489	9.27292968
C	20.48275471	-7.88552038	10.12506121
C	19.29579744	-7.32551210	9.66802452
C	18.17121006	-6.31717105	7.53309924
C	19.93404855	-6.60029172	6.15979246
H	22.36638352	-7.80153493	7.25665577
H	20.56789155	-8.20046244	11.16072670
H	18.43967777	-7.19995829	10.32316173

C	20.51314441	–5.59175281	1.64777234
C	21.25036050	–6.15873220	2.71158510
C	22.55763839	–6.60554486	2.52388376
C	23.11292328	–6.47283700	1.25048156
C	22.37884485	–5.90674937	0.19053650
C	21.07010235	–5.45952178	0.37627919
C	19.19980972	–5.24269630	2.18728190
C	20.37474562	–6.14472049	3.88201454
H	23.11428708	–7.04154247	3.34743166
H	24.12936001	–6.81182985	1.07038139
H	22.84234681	–5.81873931	–0.78821234
H	20.49504115	–5.02252522	–0.43398407
C	14.67443728	–5.08901996	7.82936166
C	13.93984840	–4.52261358	6.76348020
C	12.63053805	–4.07957516	6.94618711
C	12.07046225	–4.21445642	8.21717460
C	12.80221590	–4.77915990	9.27947354
C	14.11271494	–5.22325727	9.09852164
C	15.98985683	–5.43595906	7.29363849
C	14.81916557	–4.53398130	5.59558146
H	12.07608121	–3.64575794	6.12002289
H	11.05225103	–3.87885924	8.39363347
H	12.33535599	–4.86894650	10.25647682
H	14.68530119	–5.65941013	9.91098869
N	16.01876456	–5.08431345	5.96558981
N	16.54694357	–4.53076637	3.22263313
N	19.17278882	–5.59129634	3.51291806

N	18.64445328	-6.14441817	6.25617125
N	14.47066038	-4.07586182	4.39223034
N	18.22184185	-4.68262691	1.47380476
N	16.96587897	-5.99567327	8.00503591
N	20.72137963	-6.60107744	5.08366278
C	23.60945765	-4.18159572	15.72439972
O	23.91509302	-4.00910759	16.89768273
C	22.52847866	-3.27119580	13.67571254
O	21.94812563	-2.34807401	13.11946248
C	24.68850420	-11.85656642	8.79634376
O	24.17530551	-12.15794630	7.72659163
C	26.34417381	-12.41259291	10.56787218
O	27.21736485	-13.16031179	10.98854338
N	25.70280003	-12.65380677	9.34203176
C	22.74688027	-5.89176630	10.97304044
C	23.34414755	-6.98461146	11.60900958
C	23.83222053	-6.79948182	12.94286439
C	23.53277791	-5.58780313	13.63728046
C	22.84985567	-4.53885979	12.97571867
C	22.50345413	-4.68706258	11.64369148
H	22.45292326	-5.96536322	9.93609048
C	24.64108044	-7.78368620	13.58872871
C	23.93504851	-5.42362975	14.98461844
H	22.02360398	-3.85887417	11.13327267
C	24.64164926	-6.43043524	15.62106865
C	25.00200182	-7.58931405	14.92415698
H	24.92665407	-6.29097169	16.65849498

H	25.57487598	-8.34499615	15.44897227
C	23.25358230	-9.86948188	9.11268713
C	24.28681559	-10.65865624	9.57183132
C	24.90874660	-10.34876988	10.80331949
C	24.51446426	-9.17820256	11.51838750
C	23.53345886	-8.29307407	10.95494766
C	22.83511835	-8.70856727	9.79895949
H	22.73719262	-10.17158996	8.20754273
C	25.90843561	-11.20823952	11.31743006
C	25.09791578	-8.93547218	12.80367146
C	26.08316047	-9.80730138	13.27383232
C	26.49351991	-10.92487441	12.54017696
H	26.56197751	-9.61928111	14.22775104
H	27.26462699	-11.58818317	12.91695963
N	22.92419888	-3.18256923	15.02061599
C	26.09181871	-13.83077195	8.55722861
H	26.89729199	-14.33559752	9.08561442
H	25.23237014	-14.49566962	8.44049296
H	26.41844992	-13.51554720	7.56351243
C	22.62043125	-1.95840298	15.76989049
H	23.54959056	-1.49979936	16.11714475
H	22.01309219	-2.20525793	16.64398706
H	22.08434654	-1.28297651	15.10708239
Zn	17.59563450	-5.33684035	4.73902031
101			
ZnPc-PDI_noD3			
C	15.12641985	-4.11704750	3.37716170

C	16.92683542	–4.22883839	2.03141790
C	14.71488722	–3.57517666	2.08089097
C	15.84506912	–3.64498063	1.23634014
C	13.50339719	–3.06027481	1.61987488
C	15.78448933	–3.20095342	–0.08442426
C	13.44545884	–2.61658232	0.29822076
H	12.63897260	–3.01002273	2.27454629
C	14.57141785	–2.68600670	–0.54306745
H	16.65722475	–3.25795780	–0.72740058
H	12.51609421	–2.20995829	–0.09108806
H	14.49164671	–2.33179500	–1.56716223
C	19.18522522	–6.93981931	8.34298417
C	20.31383530	–7.01388539	7.49725801
C	21.52555764	–7.53211735	7.95398565
C	21.61119403	–7.96502678	9.28398541
C	20.46897033	–7.89266766	10.12138141
C	19.25730827	–7.38613364	9.66482348
C	18.10383257	–6.36120674	7.54998512
C	19.90291747	–6.47594856	6.20110030
H	22.38494631	–7.58397074	7.29223596
H	20.54931177	–8.25186471	11.14310626
H	18.38660013	–7.34255695	10.31153332
C	20.49886848	–5.22530691	1.75017598
C	21.25112167	–5.79453840	2.80209670
C	22.58897886	–6.14569582	2.62127880
C	23.15889635	–5.91561637	1.36884487
C	22.40993496	–5.34769451	0.32114068

C	21.07166168	–4.99611063	0.49886355
C	19.15521881	–4.98625855	2.27807983
C	20.35352624	–5.89147070	3.95337760
H	23.16039736	–6.58402624	3.43349669
H	24.19882357	–6.17882141	1.19608375
H	22.88503532	–5.18198342	–0.64188331
H	20.48778925	–4.55825268	–0.30472448
C	14.52894164	–5.37010998	7.82915221
C	13.77875335	–4.80346175	6.77440702
C	12.43937510	–4.45529741	6.94991918
C	11.86549142	–4.68505497	8.20051065
C	12.61252729	–5.24968021	9.25138867
C	13.95217701	–5.59866656	9.07874644
C	15.87432563	–5.60776867	7.30495558
C	14.67927640	–4.70561892	5.62536281
H	11.87004753	–4.02038743	6.13439873
H	10.82420368	–4.42471596	8.36943112
H	12.13469553	–5.41523087	10.21310350
H	14.53384409	–6.03416959	9.88521167
N	15.90431405	–5.19523897	5.99531968
N	16.44429657	–4.48738361	3.28916933
N	19.12607792	–5.39885299	3.58457757
N	18.58625219	–6.10608393	6.29127311
N	14.32425334	–4.21549194	4.43615244
N	18.15657143	–4.45417140	1.57109980
N	16.87224798	–6.13603563	8.01098614
N	20.70677058	–6.37967725	5.14113661

C	23.72988305	-4.18679728	15.80890393
O	24.07552480	-4.03144818	16.97331809
C	22.56158764	-3.25823033	13.81815224
O	21.94642649	-2.33469874	13.30155205
C	24.74716228	-11.69866247	8.68533253
O	24.22040877	-11.98049275	7.61700526
C	26.43836662	-12.27295742	10.41566932
O	27.32823124	-13.01878412	10.80342511
N	25.78025258	-12.49492585	9.19531715
C	22.72382528	-5.82570831	11.05991108
C	23.36877577	-6.91813521	11.64803920
C	23.89638565	-6.75024235	12.97034086
C	23.60067273	-5.55710895	13.69919753
C	22.87686461	-4.50752374	13.08321003
C	22.48296454	-4.63847103	11.76300407
H	22.39363382	-5.88365761	10.03306358
C	24.74082940	-7.73283153	13.57109864
C	24.04748893	-5.41016807	15.03475539
H	21.96962536	-3.81011068	11.28650758
C	24.79191834	-6.41662520	15.62721473
C	25.14494799	-7.55659005	14.89672739
H	25.11167587	-6.29168725	16.65630303
H	25.74770226	-8.31205735	15.38716474
C	23.29227066	-9.73841833	9.07272880
C	24.34223347	-10.52526695	9.49660819
C	24.97907273	-10.23540911	10.72505740
C	24.57935044	-9.08718391	11.47399286

C	23.57084279	-8.20483006	10.95174021
C	22.86363926	-8.60083774	9.79261777
H	22.76877582	-10.02546566	8.16691573
C	25.99993951	-11.09273700	11.20070112
C	25.18836683	-8.86425180	12.75154930
C	26.19319097	-9.73363896	13.18341138
C	26.60358237	-10.82978158	12.41872110
H	26.68798106	-9.55971125	14.13175098
H	27.38977006	-11.49110423	12.76665456
N	23.00514872	-3.18621622	15.14886585
C	26.17644473	-13.64891231	8.38086199
H	26.99853233	-14.14647587	8.89027780
H	25.32903696	-14.32926094	8.26428418
H	26.48396418	-13.31073137	7.38859702
C	22.70785165	-1.97789325	15.92565302
H	23.63950476	-1.50554205	16.24697903
H	22.13328184	-2.24372547	16.81622452
H	22.13870485	-1.30598907	15.28723771
Zn	17.51462990	-5.29739659	4.78932381